NASA/TM—2012-217823

Contamination Control Assessment of the World's Largest Space Environment Simulation Chamber

Aaron Snyder, Michael W. Henry, and Stanley P. Grisnik
Glenn Research Center, Cleveland, Ohio

Stephen M. Sinclair
Sierra Lobo, Inc., Fremont, Ohio

December 2012

NASA STI Program . . . in Profile

Since its founding, NASA has been dedicated to the advancement of aeronautics and space science. The NASA Scientific and Technical Information (STI) program plays a key part in helping NASA maintain this important role.

The NASA STI Program operates under the auspices of the Agency Chief Information Officer. It collects, organizes, provides for archiving, and disseminates NASA's STI. The NASA STI program provides access to the NASA Aeronautics and Space Database and its public interface, the NASA Technical Reports Server, thus providing one of the largest collections of aeronautical and space science STI in the world. Results are published in both non-NASA channels and by NASA in the NASA STI Report Series, which includes the following report types:

- TECHNICAL PUBLICATION. Reports of completed research or a major significant phase of research that present the results of NASA programs and include extensive data or theoretical analysis. Includes compilations of significant scientific and technical data and information deemed to be of continuing reference value. NASA counterpart of peer-reviewed formal professional papers but has less stringent limitations on manuscript length and extent of graphic presentations.

- TECHNICAL MEMORANDUM. Scientific and technical findings that are preliminary or of specialized interest, e.g., quick release reports, working papers, and bibliographies that contain minimal annotation. Does not contain extensive analysis.

- CONTRACTOR REPORT. Scientific and technical findings by NASA-sponsored contractors and grantees.

- CONFERENCE PUBLICATION. Collected papers from scientific and technical conferences, symposia, seminars, or other meetings sponsored or cosponsored by NASA.

- SPECIAL PUBLICATION. Scientific, technical, or historical information from NASA programs, projects, and missions, often concerned with subjects having substantial public interest.

- TECHNICAL TRANSLATION. English-language translations of foreign scientific and technical material pertinent to NASA's mission.

Specialized services also include creating custom thesauri, building customized databases, organizing and publishing research results.

For more information about the NASA STI program, see the following:

- Access the NASA STI program home page at *http://www.sti.nasa.gov*

- E-mail your question to *help@sti.nasa.gov*

- Fax your question to the NASA STI Information Desk at 443–757–5803

- Phone the NASA STI Information Desk at 443–757–5802

- Write to:
  STI Information Desk
  NASA Center for AeroSpace Information
  7115 Standard Drive
  Hanover, MD 21076–1320

NASA/TM—2012-217823

Contamination Control Assessment of the World's Largest Space Environment Simulation Chamber

Aaron Snyder, Michael W. Henry, and Stanley P. Grisnik
Glenn Research Center, Cleveland, Ohio

Stephen M. Sinclair
Sierra Lobo, Inc., Fremont, Ohio

Prepared for the
27th Space Simulation Conference
cosponsored by the IEST, NASA, CSA, AIAA, ASTM, and JHU/APL
Annapolis, Maryland, November 5–8, 2012

National Aeronautics and
Space Administration

Glenn Research Center
Cleveland, Ohio 44135

December 2012

Level of Review: This material has been technically reviewed by technical management.

Available from

NASA Center for Aerospace Information
7115 Standard Drive
Hanover, MD 21076–1320

National Technical Information Service
5301 Shawnee Road
Alexandria, VA 22312

Available electronically at http://www.sti.nasa.gov

Contamination Control Assessment of the World's Largest Space Environment Simulation Chamber

Aaron Snyder, Michael W. Henry, and Stanley P. Grisnik
National Aeronautics and Space Administration
Glenn Research Center
Cleveland, Ohio 44135

Stephen M. Sinclair
Sierra Lobo, Inc.
Fremont, Ohio 43420

Abstract

The Space Power Facility's thermal vacuum test chamber is the largest chamber in the world capable of providing an environment for space simulation. To improve performance and meet stringent requirements of a wide customer base, significant modifications were made to the vacuum chamber. These include major changes to the vacuum system and numerous enhancements to the chamber's unique polar crane, with a goal of providing high cleanliness levels. The significance of these changes and modifications are discussed in this paper. In addition, the composition and arrangement of the pumping system and its impact on molecular back-streaming are discussed in detail. Molecular contamination measurements obtained with a TQCM and witness wafers during two recent integrated system tests of the chamber are presented and discussed. Finally, a concluding remarks section is presented.

Introduction

This paper presents aspects of contamination control in the Space Power Facility (SPF) thermal vacuum test chamber. This test chamber is the largest chamber in the world capable of providing an environment for space simulation. SPF is located at the NASA Glenn Research Center's Plum Brook Station near Sandusky, Ohio.

The thermal vacuum chamber has a rich heritage, in large part by being able to accommodate a wide range of testing environments, ranging from ambient pressures and temperatures of launch, through ascent, to the extreme low pressures and widely fluctuating temperatures occurring in space. The facility was designed and constructed to test both nuclear and non-nuclear space hardware in a simulated low-Earth-orbit environment. Although the facility was designed for testing nuclear hardware, only non-nuclear tests have been performed throughout its history. Some of the test programs that have been performed at the facility include high-energy experiments, rocket-fairing separation tests, Mars Lander system tests, deployable Solar Sail tests and International Space Station hardware tests. The large chamber size accommodates both small and bulky test article configurations. With the additions of two new testing facilities within SPF, adding world-class vibration and acoustic capability, the thermal vacuum chamber is the cornerstone of a comprehensive facility for conducting a variety of ground-based tests.

The SPF Facility layout, shown in Figure 1, is ideal for performing multiple test programs. The facility has two large high bay areas adjacent to either side of the vacuum chamber. The advantage of having both areas available is that it accommodates the undertaking of two complex test programs. For example, one test can be prepared in a high bay while another test is being conducted in the vacuum test chamber. Large chamber doors provide access to the test chamber from either high bay. The test chamber is enclosed inside a larger concrete vacuum chamber.

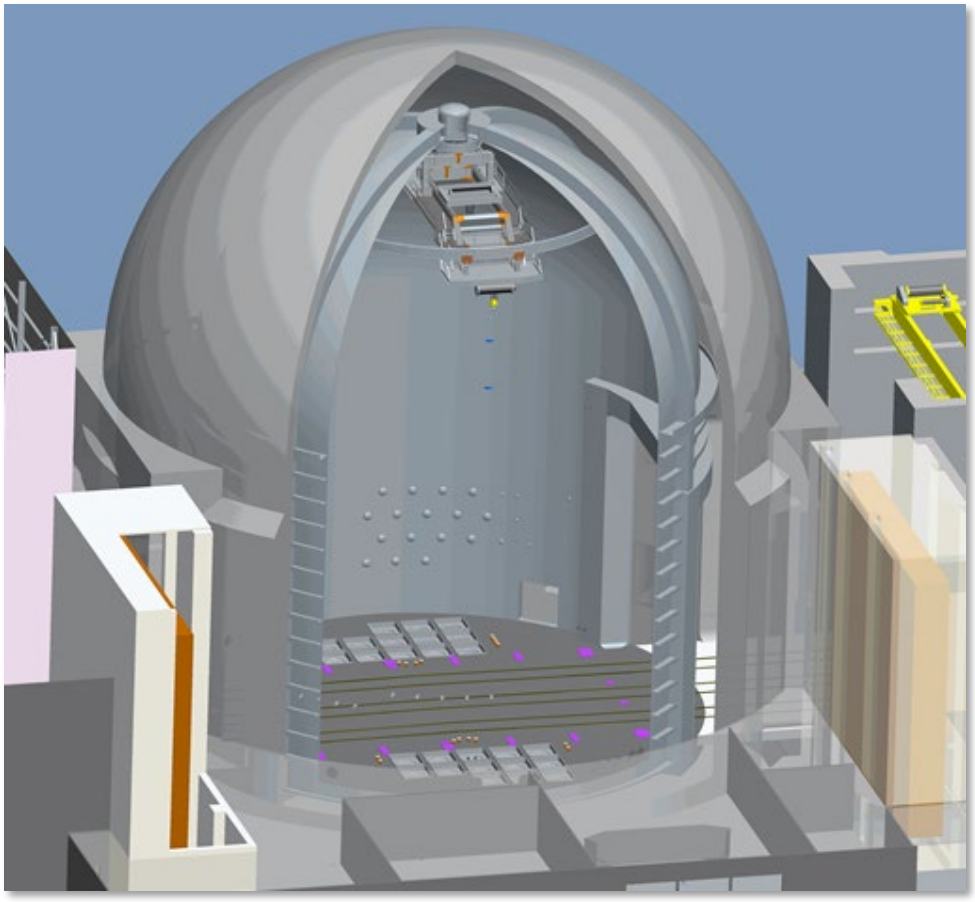

Figure 1.—Solid model view of SPF's thermal-vacuum chamber.

For thermal-vacuum testing, the SPF has a cryoshroud that is being structurally modified for use in a vertical configuration, as illustrated in Figure 2, rather than in a horizontal Quonset-hut like configuration as most recently deployed. The vertical orientation allows it to enclose tall test articles. In order to provide access in this orientation, it will be able to open and close at either end in a clam-shell fashion. The thermal environment range provided by the cryoshroud will be approximately –157 to 66 °C (–250 to 150 °F). Background contamination produced by the chamber can significantly degrade the inherent capability of even a well-designed and contaminant-free shroud to provide a clean environment. To minimize background contamination, significant changes and modifications were made to improve vacuum chamber performance. For many of these improvements, emphasis was placed on meeting requirements of a wider customer base, particularly those having stringent contamination control requirements. These alterations include major changes to the large and complex vacuum-pumping system and numerous enhancements to the chamber's unique polar crane. In addition to hardware and material improvements, a thorough cleaning of the test chamber was performed in the year 2007 by a commercial vendor to remove existing contaminants such as diffusion pump oil. Diffusion pumps are not a component of the current pumping system. Recently, two system integration tests were conducted at high vacuum, which provided key opportunities to establish chamber background levels of molecular contamination. It was intended that contamination results obtained during these system integration tests serve not only as a basis to characterize empty chamber cleanliness but also to establish a reference characterization to judge contamination issues pertaining to testing with the cryoshroud in place. It should be emphasized that the test chamber results presented in this paper are for vacuum testing without the cryoshroud placed in the chamber.

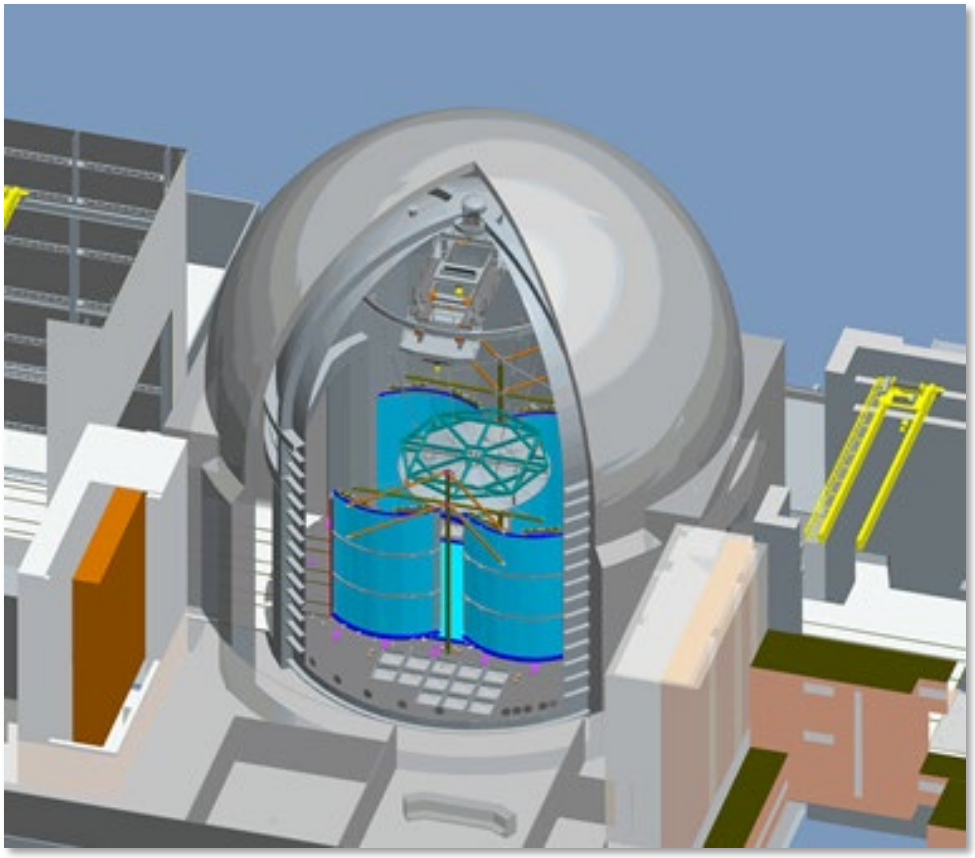

Figure 2.—Solid model view of the thermal-vacuum chamber with cryoshroud in place.

The main body of this paper is outlined as follows. First, brief descriptions of the concrete enclosure and test chamber are given. Second, the composition and arrangement of the current pumping systems are reviewed. This review is centered on the design's inherent impact on contamination control and methods used that minimize molecular back-streaming. Next a broad description of the polar crane is presented to provide insight into the scope of modifications made to this complex unit. Details of the significant changes made to the crane to reduce contamination are described. Recent empty-chamber molecular contamination measurements, obtained during two high-vacuum integrated system tests (IST) are presented and discussed. These data were obtained using a residual gas analyzer (RGA), a thermoelectric quartz crystal microbalance (TQCM), and witness wafers. A concluding remarks section includes a discussion of the significance of these results.

Concrete Enclosure and Test Chamber

The concrete chamber enclosure serves not only as a radiological shield but also as a primary vacuum barrier from atmospheric pressure. At 39.6-m. (130 ft) in diameter and 45.7-m (156 ft) in height, this chamber was designed to withstand atmospheric external pressure while operating internally at vacuum conditions. The concrete thickness varies from 1.8 m (6 ft) to 3 m (10 ft) and contains a leak-tight steel containment barrier embedded within. The chamber's door openings are 15.2- by 15.2-m (50- by 50-ft) and have inflatable seals. The annular region between the concrete enclosure and the aluminum test chamber is pumped down to a nominal pressure of 2.67 kPa (20 torr) during vacuum test operation.

The aluminum test chamber is a high-vacuum aluminum plate vessel 30.5 m (100 ft) in diameter and 37.2 m (122 ft) in height. Designed for a maximum external pressure of 17.2 kPa (2.5 psig) and maximum internal pressure of 34.5 kPa (5.0 psig), the chamber shell is constructed of type 5083 aluminum which

has a type 3003 aluminum cladding on the interior surface. The type 3003 alloy was selected because of its low neutron absorption cross-section and high corrosion resistance. The door openings of the test chamber are 15.2- by 15.2-m in size and have double door seals, with a guard-vacuum system between seals, to minimize annulus-to-chamber leakage.

Before each IST, the readily accessible areas of the chamber were cleaned using a commercial surfactant and rinsed thoroughly with distilled water. These areas included: the chamber floor; lower chamber wall and penetrations; door-pocket ledges; scavenger plates and wells; cryopump wells; and polar-crane walkways, handrails, and stairs.

SPF Vacuum Pump System

Evacuating very large space simulation chambers in reasonable times requires using high pumping speed mechanical pumps. These pumps are typically oil-filled. The migration of oil from these pumps back toward the chamber must be prevented to avoid contaminating sensitive hardware. There are numerous ways to contaminate equipment inside a vacuum chamber through the mechanical pumping system. If the mechanical pump evacuates its inlet piping below the viscous flow range, the pump oil will migrate toward the vacuum chamber. For example, suppose on shutdown that the inlet piping is vented to atmosphere near the mechanical pump inlet, and the piping contains oil from a previous operation in the molecular flow range. In this case, the air flow will provide a means to carry the oil further up the piping. In other instances, a mechanical pump's structural integrity might become compromised, or a drive belt might fail, allowing air and oil to flow backward in the vacuum piping. Roots rotary lobe pumps, such as used at the SPF, can also cause oil migration issues if not properly protected. Glenn Research Center became aware of oil migration issues during the early 1980s testing of electric propulsion devices for space applications. It was noted that cracked mechanical pump oil was found inside the discharge chambers of ion thrusters after long test periods, Reference 1. The oil also showed up in the grain structure of refractory metals operated at high temperatures inside the chambers, Reference 2. The SPF has incorporated the same safeguard features that are known to prevent this type of contamination as are used on other NASA Glenn chambers.

There are four methods frequently employed to eliminate backstreaming from a roughing system. First, a cryogenically cooled oil vapor trap can be installed upstream of the roughing pump. The trap must be operated in such a manner to prevent it from warming and releasing the trapped oil when the piping is below the viscous flow range. Second, A molecular sieve can be installed upstream of the roughing pump. The molecular sieve must be baked out often and properly to prevent oil backstreaming. Third, is the use of an oil free roughing pump which completely eliminates the oil. The fourth method is the use of an inert gas purge that keeps the roughing pump inlet piping in the viscous flow range over a minimum of ten pipe diameters upstream of the oil source to ensure a uniform, viscous gas flow to the pump. The inert gas supply must be reliable and/or interlocked to prevent backstreaming. Of these methods, the best choice seems to be the oil free pumps because they completely remove the oil. However they become impractical on large vacuum chambers due to their current size limitations and the desire to evacuate the chamber as quickly as possible. The SPF chamber is so large that a conventional evacuation beginning with roughing pumps to reduce the chamber pressure from ambient pressure 101.3 kPa (760 torr) to around 1.33 kPa (10 torr) would take six days using an oil-filled 354-L/s (750-cfm) rotary piston pump. Oil-free pumps would take longer.

The SPF has multiple vacuum systems. The main rouging system is used to evacuate the chamber to approximately 2 Pa (0.015 torr). The high vacuum system uses 10 cryogenic and five turbomolecular pumps. Each of these systems has its own roughing train.

The SPF main vacuum pumping train consists of four stages of Roots type rotary-lobe pumps (Roots blowers), followed by one stage (fifth stage) of rotary piston pumps. The pumps are arranged and operate as follows. The first stage is attached to the chamber by way of piping having a composite length consisting of: a 29-m (95-ft) section of 0.91-m (3-ft) diameter piping connected in series with a 47.5-m (156-ft) section of 1.2-m (4-ft) diameter piping. The first stage is comprised of four 7,100 L/s (15,000-cfm) Roots blowers in

parallel. The stage exhausts to the atmosphere during the chamber evacuation from atmospheric pressure 101.3 kPa (760 torr) to 64 kPa (480 torr). At this lower pressure, the second stage is started. The second stage consists of two 8500 L/s (18,000-cfm) Roots blowers in parallel. The first stage evacuates the chamber down to 32 kPa (240 torr) and exhausts into the second stage, which exhausts to atmosphere. At 32-kPa chamber pressure, the third stage is started. The third stage consists of two 4,700-L/s (10,000-cfm) Roots blowers in parallel. As the chamber is evacuated to16 kPa (120 torr), the third stage exhausts to atmosphere. At 16 kPa the fourth stage is started. The fourth stage consists of two 2600-L/s (5500-cfm) Roots blowers in parallel. As the chamber is evacuated to 12 kPa (90 torr), the fourth stage exhausts to atmosphere. At this level the fifth stage is started. The fifth stage consists of six Beach-Russ rotary piston pumps each with a 354-L/s (750-cfm) pumping speed.

At a chamber pressure of 2.67 kPa (20 torr), the pumping system is isolated from the annulus region, a volume of 22,700 m^3 (800,000 ft^3), and only the inner, high vacuum chamber, having a volume equivalent to the annulus, is evacuated down to 4 Pa (0.030 torr). At 4 Pa the compound turbomolecular high-vacuum pumping system is started. It is interesting to note that at this pressure, the turbo pumps provide an additional 10 percent in pumping capacity to the roughing system. At 1.6 Pa (0.012 torr) the increase is approximately 25 percent.

At a chamber pressure of 1.6 kPa, the roughing system is isolated from the chamber and cryopumps are operated along with the turbomolecular pumps. One cryopump, constructed without charcoal surfaces, is opened to the chamber to remove the remaining gas load from the chamber. The charcoal surfaces have been removed to aid in the removal of water vapor during regeneration of this pump. In the 0.1 Pa ($\sim 10^{-3}$ torr) range, the remaining pumps are then brought online. In aggregate, a chamber base pressure of 17.3 μPa (1.3×10^{-6} torr) can be obtained in less than 12 h.

Oil contamination occurring during high vacuum operation of large vacuum systems can be eliminated by the use of cryogenic and/or magnetically levitated turbomolecular pumps. The SPF uses both to obtain high vacuum levels.

For the high vacuum system, the five 2400 L/s magnetically levitated, compound turbomolecular pumps are backed by an oil free rotary lobe blower and an oil free mechanical reverse claw pump. Oil-free pumps can easily be found in the sizes required for this system. While this system operates, the roughing lines are in the molecular flow range. The ten 1.22 m (48 in.) cryopumps use a roughing system consisting of three Kinney oil-filled mechanical pump/blower packages for regeneration.

Concerns have been raised about oil backstreaming at the SPF. It is important to note that diffusion pumps are no longer used at the SPF. The facility originally used diffusion pumps, which operated with DC705 oil. When operation was with diffusion pumps, the issues of back streaming were more pronounced than they at present. Methods were developed to measure the backstreaming rates during diffusion pump operation as presented in Reference 3. Now, as mentioned above, the turbomolecular pumping system uses oil-free pumps to eliminate oil backstreaming. The oil-filled roughing pumps on the cryopump regeneration system utilize several methods to prevent oil backstreaming. The first method is the use of molecular sieves for each pump package. The second is a nitrogen gas purge at the inlet of the molecular sieve and the third is a nitrogen gas purge at the cryopump. The piping between the cryopumps and the roughing pumps is 15.24-cm (6-in) diameter and approximately 46-m (150- ft) long. This length is equivalent to 300 pipe diameters, and for which the flow is viscous due to the gas purge at the cryopumps. The purge at the molecular sieve keeps the roughing pump inlet piping in viscous flow, preventing backstreaming, when the pump is isolated from the header piping. Corresponding to this latter case, the distance between the pump and the isolation valve is equivalent to 15 pipe diameters. The roughing pumps utilize rotation sensors that detect a loss of pump rotation. In the event of a pump, motor, or belt failure, the affected pump is automatically isolated and shutdown. This prevents any back flow of oil-laden gas.

A failure of both gaseous nitrogen purges would allow backstreaming to occur if the molecular sieve was not present. To ensure the molecular sieve does not allow oil contamination to enter the vacuum chamber, it is baked out by heating and purging after every system operation. A molecular sieve that is not baked out often will saturate and allow oil to continue up the piping. It is highly unlikely that a failure

of the gaseous nitrogen system would go unnoticed as it is an integral part of the regeneration process due to the cryopumps location inside the vacuum annulus, to be explained below.

Regeneration of a cryopump is typically begun by turning off the compressor, halting liquid nitrogen (LN_2) flow, and letting the pump warm. The condensates vaporize, and the pressure rises as gases are generated. At an internal pressure of approximately 20 kPa (3 psi), the gases exit through a relief valve on the cryopump body. Because the SPF pumps operate in the 2- to 3.5-kPa (15 to 26 torr, or 0.3 to 0.5 psi) range, the relief valve will open if their internal pressure is allowed to rise to 20 to 35 kPa (3 to 5 psi), causing gases to be dumped into the vacuum annulus. This dumping is undesired as the relief valve would need to be reseated. Manually reseating the relief valve would require venting the chamber and annulus to atmosphere, interrupting test operations. Instead, a method is required that prevents the gases from entering the vacuum annulus avoiding the issues caused by the relief valve not re-seating properly when regeneration is completed.

Regenerating the pumps while simultaneously evacuating them to remove the evolved gases reduces the convection heat transfer between the internal shrouds and the pump body. The regeneration time would take more than 24 h. If the roughing system is used in a cyclic manner, to remove the gasses before a pressure of 20 kPa (3 psi) is reached, the regeneration time is increased due to the gas cooling caused by each pressure reduction cycle. Again, the regeneration time would be more than 24 h.

The chosen method is regeneration using a gas purge with dry nitrogen to warm the pumps while evacuating with the roughing system. The pressure is kept around 0.5 kPa (4 torr) during this timeframe. This method regenerates the pumps in a more reasonable time because appreciable convective heat transfer occurs at this pressure level. Remaining below 0.67 kPa (4.7 torr) also removes moisture accumulated on the cold surfaces by sublimation rather than by melting followed by evaporation. It takes approximately 7 h for regeneration using this method. Purging with heated nitrogen at 0.5 kPa does not further reduce the regeneration time to any appreciable extent. To enable this rapid regeneration, the use of the GN2 system is required. Furthermore the GN_2 system must be maintained to ensure availability. Regeneration is performed manually due to its complexity, and to ensure that a loss of nitrogen is detected. Finally, control logic upgrades isolate the pumps if they drop below the viscous flow regime.

For the chamber roughing system, starting at the last stage, there is approximately 9 m (30 ft) of piping between the roughing pumps and the fourth stage Roots blowers. Due to the gas compression from the Roots blower stages, this piping stays in the viscous flow regime during the entire chamber evacuation down to cryopump crossover at 1.6 Pa (0.012 torr). It would take an additional 30 min of pumping on the chamber to reduce the roughing pump inlet-piping pressure to 2.9 Pa (0.022 torr), which would be necessary in order to exit the viscous flow regime. The minimum vacuum level possible by the Roots blowers is approximately 0.53 Pa (0.004 torr), limited by chamber leakage. A chamber pressure of 0.5 Pa (0.00375 torr) must be reached to allow back streaming from the blower inlet piping due to non-viscous flow. The only possible way to induce oil backstreaming would be to operate the high vacuum system while the roughing system is still open to the chamber. As with all vacuum systems, it is standard practice to isolate the roughing system from the chamber before the high vacuum system is used. It is for good reason. When backstreaming of oil occurs, the base pressure of the chamber becomes higher than normal. Planned control logic upgrades will prevent the possibility of being able to open the high vacuum valves when the roughing-line vacuum valve to the chamber is still open.

The entire length of inlet piping, approximately 76.1 m (251 ft) between the chamber and the first stage pumps, greater than 60 pipe diameters, will be in the viscous flow range during the entire evacuation. If any oil leaked through the carbon seals of the Roots Blower stages, the viscous flow from the chamber would prevent backstreaming. The control logic monitors the roughing train pressure to ensure the pumps operate as intended, and eliminate the possibility of a pump failure of the type that would allow air and pump oil to enter the piping. The roughing pumps are isolated from the system by valves approximately 1.5 m (5 ft) above their inlets. In the event that the roughing pumps are operated while isolated from the system, at most 1.5 m of piping will be contaminated with oil. Upcoming logic additions to the control system will isolate a pump should it, its motor, or drive belt fail. This isolation feature eliminates the possibility of air and oil entering the piping through a non-operating pump.

Because the Roots blowers are started first for a chamber evacuation, and because they must be open to the chamber at the start of evacuation or pump damage will occur, the pumping system is not dead-headed at the chamber isolation valve. Avoiding dead-heading also prevents the possibility of contaminating the piping before a chamber evacuation is started, because dead-heading the pumping system places the pipe flow into molecular regime. The longer the flow remains in this regime, the further oil can migrate up the piping toward the chamber. As the distance between the oil and chamber drops below 10 pipe diameters, a gas purge becomes less effective in keeping the oil out of the chamber.

Polar Crane Contamination Control Implementation

It is important to review the main reasons crane modifications were useful and needed. First, the crane had been neglected over the years and exhibited visibly evident sources of contaminants such as leaked greases and oils deposited on surfaces, leaking seals, degradation of adhesives, and disintegration of electrical resistor banks. This condition was not acceptable for customers having sensitive hardware. Second, the crane needed to be lowered to repair critical cracks in its structure. Third, due to its essential utility, reinstallation will be necessary after each crane removal, and reinstallation is a complicated procedure accompanied with risks. Fourth, crane utilization followed by its removal imminent to testing is not a viable option due to the difficulty and risks associated with lowering the crane with a test article and cryoshroud in the chamber. The picture presented in Figure 3 shows the polar crane bridge as it was being lowered for repair in 2007. In the case of reinstalling lifting hardware, such as a hoist, the hoist must be load tested before being used again for critical lifts. It would be problematic to load test a hoist if a valuable test article or cryoshroud is present in the chamber. Lowering the crane to make structural repairs presented the opportunity to upgrade the crane in additional areas. In addition to the contamination control upgrades, upgrades were made to the electrical controls, gears, motors, and brakes to improve safety and operating performance.

Figure 3.—Lowering of the polar crane bridge.

The unique polar crane is a large structure. The polar crane is described below in some detail to illustrate that it is a very complex system of hardware, and to provide a perspective on the scope of the modifications made to the crane to mitigate contamination. These steps included cleaning, stripping existing coatings and applying low-outgassing surface coatings, utilizing improved low-vapor-pressure fluorocarbon polymer lubricants, installing improved or redesigned seals, replacing bearings, and modifying gear-box vents. To meet crane safety standards, it was necessary to affix labels to the underside of the bridge specifying the hoists' load capacities. This was done by applying "hot-sprayed" Teflon (DuPont) coatings to signage, having low-outgassing characteristics, to form text. In addition, all crane components including the bridge were cleaned using a multistep process involving commercial specialty cleaners designed specifically to remove greases, oils, siloxsanes, adhesives, and other hydrocarbon contaminants. Next a description of the crane is given, followed by an outline presenting these key modifications.

The crane's major utility is lifting and transporting large articles. It is ceiling mounted as shown in Figure 4. It is approximately 37 m (122 ft) above floor level and supported by two circular tracks welded to the chamber dome. The inner track is 3.2 m (10.5 ft) in diameter and the outer track is 9.9 m (32.5 ft) in diameter. The polar crane bridge can rotate 360° about the axis of the chamber. The bridge crane is equipped with a 20-ton main-hoist trolley. The trolley can travel in a radial direction, allowing its hoist to be placed, at any desired circumferential orientation, as far as 5.8 m (19 ft) from the center of the chamber. A 10-ton auxiliary hoist is affixed to the outer extremity of the crane bridge. The maximum height of the main hook above the chamber floor is approximately 30.5 m (100 ft). The combined weight of the bridge, trolley, and hoists is approximately 18,000 kg (40,000 lb).

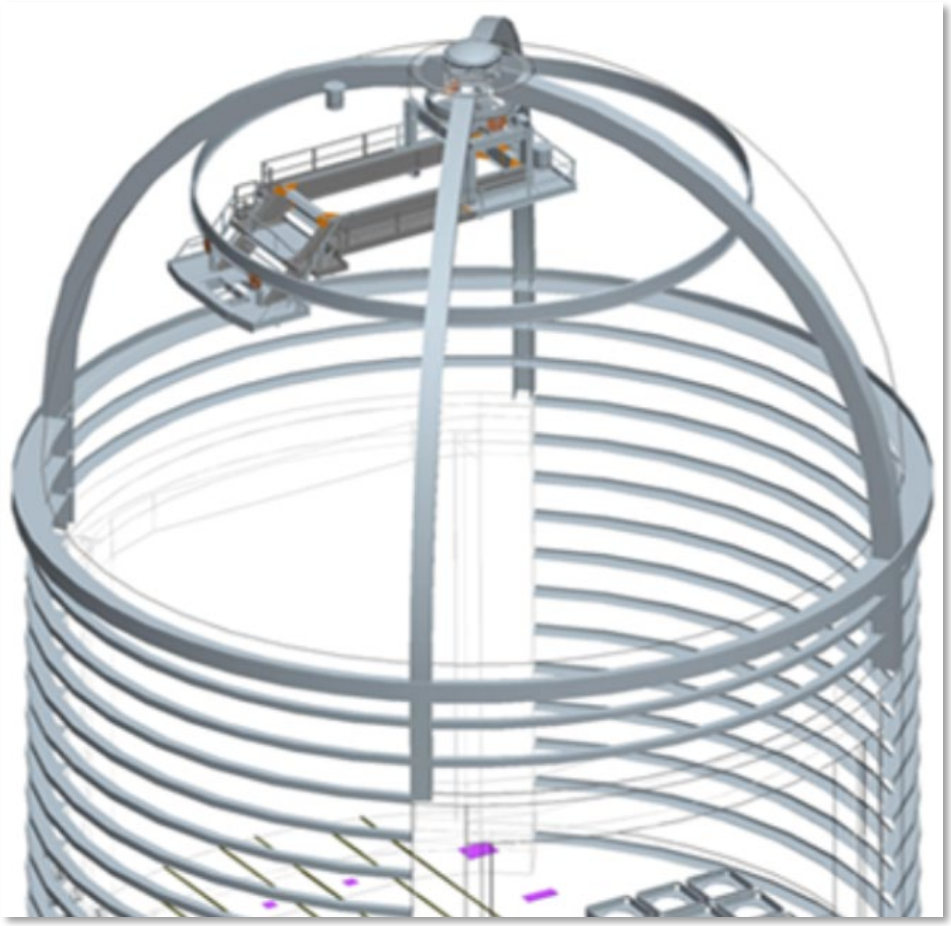

Figure 4.—Positioning of polar crane bridge at top of chamber.

The crane bridge structure is composed of aluminum. It has a type 3003 aluminum cladding. It is approximately 15 m (50 ft) in length, 6 m (20 ft) wide, and 6 m (20 ft) high. It is comprised of four deck levels connected by large structural beams and plate members. Structural members are joined either by welds and/or bolted fasteners. The top deck is essentially an access deck. It is positioned immediately below the inner bridge rail track. A 1.8 m (6-ft) port in the test chamber dome provides access to this deck from the annulus space, which is facilitated by a bridge-mounted ladder. From this level, steps lead down to a large second level comprising the bulk of the bridge. This level contains the trolley rails and their support structure. The rails are raised from adjacent walkway decking, which allows passage on either side of the trolley system. Outward and proximate to the chamber dome, the third and fourth levels are smaller and accessed on either side by steps leading down from the walkways. The bridge control cabinets are on the third level of decking. The fourth level allows access to the outer rail bridge wheels and their drive motors. Access to the auxiliary hoist, which is mounted below the lowest level, is gained by openings in the deck.

The crane is comprised of five main power subassemblies: 1) bridge drive units; 2) 10-ton hoist; 3) 20-ton hoist; 4) trolley drive system; and 5) electrical system. The bridge drive unit subassembly consists of four electric motors that move the bridge in a circular path. A complete drive unit is made up of a motor, a disc brake, and a gear reducer all enclosed in a single housing suspended below the outer track. These units, positioned at the outermost bridge corners, are attached to the bridge in sets of two. The 10-ton hoist subassembly is made up of an electric drive motor, redundant load brakes, and a gear reducer. The 20-ton crane employs a 22-kW (30-hp) electric motor with a double shaft extension. One end of the shaft is coupled to a shoe brake and tachometer, while the opposite end of the shaft is coupled to a gear reducer. The complete trolley hoist assembly is mounted on a trolley platform that is driven along a set of tracks. The trolley is driven by a 0.56-kW (0.75-hp) electric motor through a separate gear reducer. The trolley is equipped with a brake mounted separate from the motor.

Material changes to the polar crane are grouped here into the following categories: 1) electrical and electronic hardware; 2) mechanical hardware; and 3) lubrication material.

The electrical modifications made to minimize contamination consisted of replacing original electrical cables, conduits, electrical boxes and relays, and control cabinets and associated electronics. As an example, some of the original steel control cabinets showed pronounced degradation. These cabinets were replaced by installing stainless-steel control cabinets housing thermoplastic junction boxes with steel bolts and nut fasteners. The original electrical wiring was replaced with Teflon and SMRL wiring. The festoon cable for the trolley was replaced with a neoprene cable.

The mechanical hardware changes made were extensive. The largest improvement consisted of electroless nickel plating many components after removing original paint coatings. The pictures presented in Figure 5, Figure 6, and Figure 7 show examples of components before being refurbished. The pictures presented in Figure 8 and Figure 9 show examples of components after being electroless nickel plated.

A list of the major hardware categories are: trolley and auxiliary hanger frames, hoist drums, trolley wheels, shank hooks, main hoist gear case cover, shaft and block covers, brake covers, bearing covers, motor casings, mounting brackets, trunions, collars, and sheaves. Modifications made to vents and seals were added to eliminate or reduce leaks and outgassing. For instance, o-ring seals were added in the main hoist block and to the 20 roller assemblies that support the bridge. The original components were unsealed and had grease fittings for packing the bearing assemblies with grease. The original fittings leaked grease, which the new sealed designs prevent. Virtual gas leaks were minimized by fully packing the bearing volumes with low-outgassing grease. Filtered vent plugs were replaced with solid pipe plugs in 20 locations. Repairs were made to the main gearbox cover to eliminate oil leaks and vents were replaced with solid plugs. The main hoist and auxiliary hoist steel wire ropes were replaced with stainless steel wire ropes. Drip pans, which had not previously been employed, were designed, fabricated, and installed below the hoists.

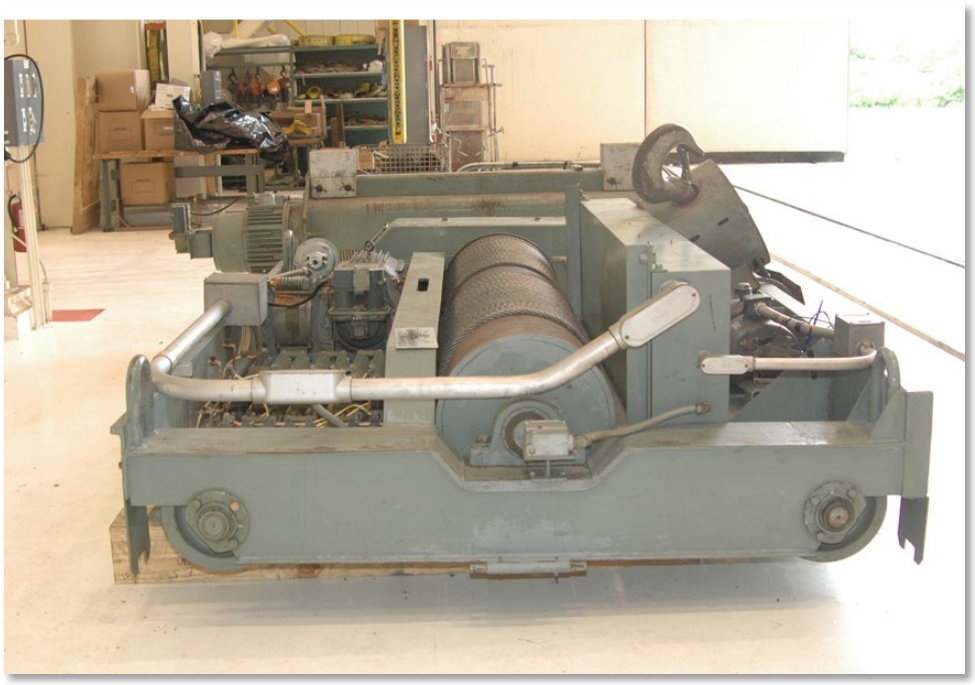

Figure 5.—Polar crane trolley before refurbishment.

Figure 6.—Original polar crane control cabinet and trolley drive motor before refurbishment.

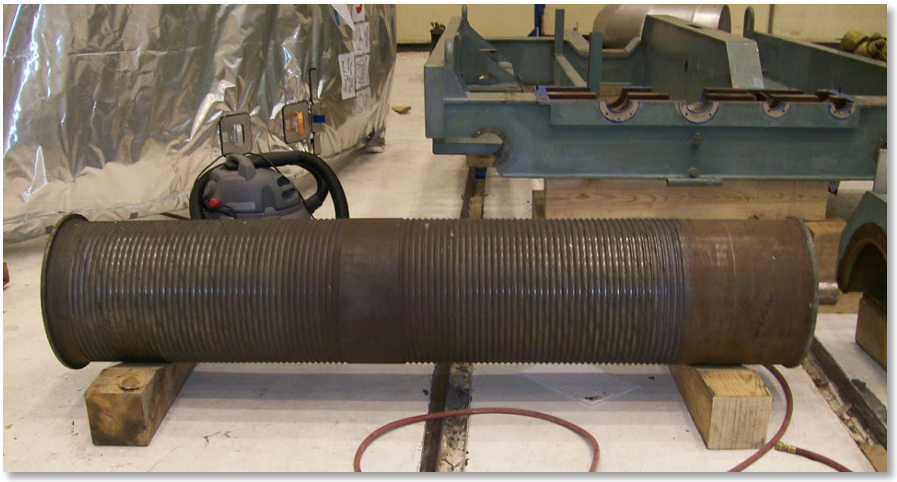

Figure 7.—Auxiliary hoist drum before electroless Ni-plating.

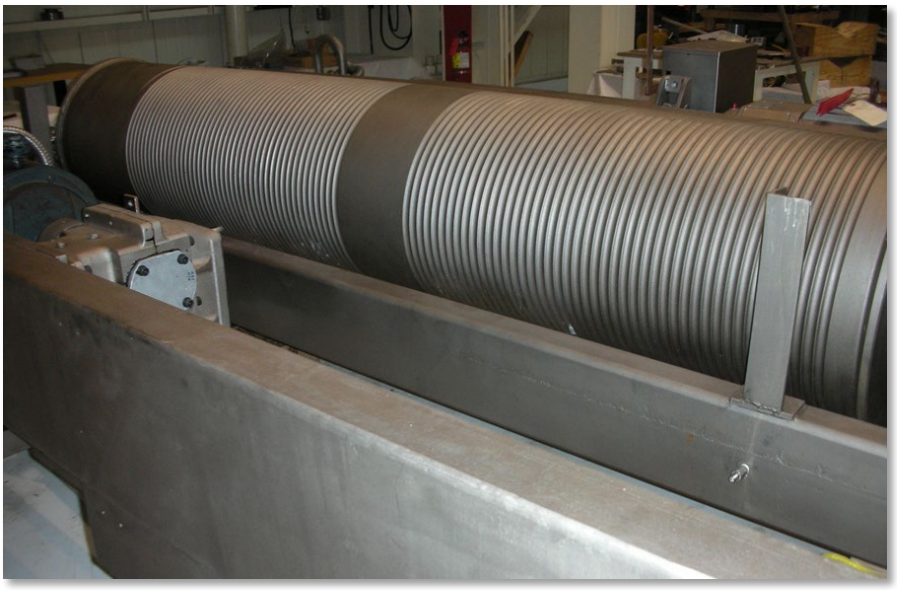

Figure 8.—Main hoist drum and trolley after electroless Ni-plating.

Figure 9.—Main hoist motor casing after electroless Ni-plating.

Figure 10.—Arrangement for applying low vapor pressure oil to hoist wire ropes.

Prior to installation, the new stainless steel wire ropes were cleaned and then re-lubricated with a low-outgassing fluorocarbon polymer lubricant. The first step in cleaning the wire ropes was performed by a commercial vendor where they had been shipped to remove the greases and oils applied during fabrication. This cleaning process comprised three cycles. Each cycle consisted of a submersion of a wire rope into a trichloroethylene (TCE) ultrasonic bath followed by raising it into the TCE vapor and spraying using distilled TCE. After this TCE cleaning process, the wire ropes were heated under vacuum at SPF to remove remaining volatile residues. Following these processes, the wire ropes were lubricated with the low-outgassing perfluoropolyether lubricant. The application of this oil used a special framework, which is shown in the picture given in Figure 10. This arrangement allowed the cleaned cable to be uncoiled from one drum, immersed for a controlled amount of time within a circular conduit containing the oil and solvent bath, and then coiled onto another drum where it remained until the bulk of the solvent evaporated. Lubrication of wire ropes is necessary to maintain their safety load margin and to ensure the ropes do not become damaged during use.

IST Results

Two recent high-vacuum ISTs were conducted in the SPF thermal-vacuum test chamber. The first test, denoted herein by IST-2010, was conducted during the period from August 9, 2010 to August 13, 2010. The second test, denoted by IST-2011, was conducted during the period from September 26, 2011 to September 28, 2011. These periods represent the durations when the test chamber was at vacuum. These ISTs were conducted to demonstrate and evaluate a number of facility functions. These include, but are not limited to, the following operations: system control procedures, movement and sealing of chamber doors, vacuum pumping system, the LN_2 and gaseous nitrogen (GN_2) system, scavenger-plate system, instrumentation performance, and data acquisition and display.

The following discussion deals with the diagnostic results obtained to measure and evaluate contaminants. This includes results obtained from witness coupons placed in the chamber to collect non-volatile residues (NVR), a RGA, and a TQCM. One goal of the ISTs was to determine if significant contamination had been introduced by adding polar-crane hardware containing materials that would tend to outgas. It was decided that the IST-2010 should be conducted without the following hardware: the polar crane trolley, main hoist, auxiliary hoist, and wire ropes. Consequently, these items were not in the chamber during IST-2010, but were in the chamber during IST-2011.

NVR Results and Discussion

NVR for each IST was collected using sets of witness coupons. The IST-2010 witness coupons consisted of three types: 1) 20-cm (8-in) diameter silicon wafers; 2) 5- by 10-cm (2- by 4-in.) gold-coated glass slides; and type-3003 aluminum sheets with dimensions 0.16- by 15.25- by 30.5-cm (1/16- by 6- by 12 in.). The IST-2011 witness coupons consisted of only the silicon wafer samples, which were supplied by Air Liquide-Balazs Analytical Services for each IST. In each case, three sets of wafer pairs were received at SPF, wrapped pair-wise face-to-face in three layers of pre-baked aluminum foil, along with a similarly wrapped control wafer and mounting brackets. The gold-coated slides and aluminum sheet were supplied by commercial vendors. The gold slides were used "as supplied". The aluminum sheets were cleaned in an ultrasonic cleaner using an aluminum-friendly detergent, and rinsed using distilled water. They were housed within a clean, air-tight aluminum box before and after each IST.

These witness coupons were placed at various locations in the chamber. In the case of IST-2010, the gold coated slides were placed at the central chamber floor, among the scavenger plate wells, on the main-door pockets ledges, and on the polar crane bridge. The aluminum sheets were placed at similar locations as the slides, and also placed adjacent to the chamber walls using hanger rods. The witness coupons were placed in sets, each set consisting of a pair of wafers. A wafer pair was held in a bracket designed for parallel positioning of the pair. The wafer placement location within the chamber was the same for each IST. The first wafer set, Set1, was placed upon the polar crane bridge, the second set, Set2, was placed upon the chamber floor, and the third set, Set3, was placed among a group of scavenger plates, as shown Figure 11.

The results for the silicon wafers are now discussed. After exposure, the sample wafers were shipped, wrapped in the original layers of foil as directed, to the supplier Air Liquide-Balazs Analytical Services. There the wafers were analyzed by TD-GC-MS (Thermal Desorption-Gas Chromatography-Mass Spectrometry) and FTIR. A set of tables, given by Table I to Table III, documents the analysis of organics obtained from the wafers. These tables list information on: 1) NVR levels for three organic boiler groups, low, medium, and high; 2) the aggregate of organic and non-organic NVR; and 3) individual levels of identified organic compounds.

Figure 11.—Silicon wafers mounted among scavenger plate wells.

For each IST the control shipping blank indicated no organic NVR level above the detectable limit, for which the value is 0.1 ng/cm^3. Table I gives information on the organic levels for wafer pairs. The total NVR levels for each wafer pair, organics and non-organics, obtained during IST-2011 from witness coupons are presented in Table II. Based on the results for the total NVR level, the molecular contamination level meets cleanliness level "A/5", References 4 and 5. This is based on the density of the predominate NVR contaminants having densities near 1 gm/cm^3. Corresponding to these cleanliness levels, spacecraft guidelines, given in Reference 6, indicate that these levels of NVR meet: *high* spacecraft sensitivity requirements for quantitative levels for *non-optics allowable* and *high* spacecraft sensitivity requirements for quantitative levels for *optics allowable* for IST-2011. Analysis by wet chemistry to measure NVR levels was performed on six of the aluminum witness plates used in IST-2010. One plate had been used as a control plate. The other five plates had been present in the chamber during the IST. The NVR for each plate was below the detectable limit of 1 µg/cm^2. This value is consistent with the wafer NVR data.

TABLE I.—ORGANIC LEVELS FOR WAFER PAIRS, ng/cm^2

Boiler range	IST-2010			IST-2011		
	Set 1	Set 2	Set 3	Set 1	Set 2	Set 3
Low C7-C10	0.9	0.7	0.7	0.7	1.8	1.3
Medium C11-C20	7.6	7.2	9.2	3.1	3.5	4.3
High > C20	13.7	26.2	41.9	11.5	16.7	13.9
Sum >= C7	22.2	34.1	51.8	15.3	22.0	19.5

TABLE II.—IST-2011 TOTAL NVR RESULTS

Location	Weight, mg	Surface density, ng/cm^2
Set 1—P.C. bridge	0.034	108.28
Set 2—Center floor	0.039	124.20
Set 3—Scavenger plates	0.036	114.65

The semi-quantitative levels of the identified organic compounds given Table III reveal that the major contaminant group is composed of phthalates such as diisononyl phthalate (DINP) and dioctyl phthalate (DEHP, DOP). This is not surprising because these constituents are found in plasticizers, which are common to many materials such as cable, wire, gaskets, seals, rubber, resins, and hose. Many of these materials are used within the annulus and to a lesser extent in the chamber. Plasticizers, often based on esters of polycarboxylic acids, are composed of complex mixtures of phthalate compounds. Used commonly in materials to soften them, plasticizers improve the flexibility and durability inherent to the original materials, but have a tendency to evaporate, and hence, readily outgas under vacuum. Such components contributing to NVR are commonly found during vacuum operation. For example, a table of NVR data from numerous vacuum tests is given in Reference 7, in which a range of phthalates are listed as significant and frequent in occurrence.

TABLE III.—IDENTIFIED ORGANIC LEVELS FOR WAFER PAIRS, ng/cm^2

Semi-quantitative levels of identified organic compounds	IST-2010			IST-2011		
	Set 1	Set 2	Set 3	Set 1	Set 2	Set 3
Diisononyl phthalate (DINP)	5.8	18.2	16.7	5.8	15.4	10
Dioctyl phthalate (DEHP, DOP)	0.7	0.8	2.9	0.9	0.4	1.4
Dinonyl phthalate	0.9	1	2.4			
2-(2-Butoxyethoxy)-ethanol	1.7	0.6	0.4	0.3	0.6	0.3
C20-C24 hydrocarbons	0.8	0.6	1.7			
C6-C10 hydrocarbons				0.2	1.8	0.9
Siloxane	0.2		1.3	0.2	0.2	0.7
Unknown (m/z: 45, 57, 73, 89, 103, 119, 161, 175, 191)	1.5	1				
Tetradecanoic acid amide		0.5	1.7			
Phthalic anhydride		0.2	0.2	0.1	0.6	0.3
Dibutyl phthalate	0.2	0.2	0.3	0.2	0.1	0.2
1ST Peak in FRYOL PCF	0.5	0.4	0.2			
Unknown(m/z: 43, 57, 70, 99, 114, 127, 141, 171)				1		
Dioctyl adipate	0.3	0.2	0.4			
Octadecanenitrile		0.3	0.2		0.2	0.2
Unknown(m/z: 43, 57, 71, 99, 137, 149)		0.4	0.4			
Dodecyl dihydrofuranone	0.3	0.2	0.3			
Alkylamide		0.7				
Unknown(m/z: 43, 77, 91, 121, 163)		0.2	0.4			
Methyldiphenyl(methyldiphenylsilyl)oxy-silane			0.6			
Butyl benzyl phthalate	0.1	0.1	0.3			
C10-C15 hydrocarbons	0.5					
Alkyl ketone		0.1	0.4			
Caprolactam		0.2	0.2			
Butyl benezenesulfonimide	0.1	0.1	0.2			
Unknown(m/z: 41, 45, 57, 71, 77, 85, 99, 117, 125,139, 157, 175)			0.4			
Hexadecannenitrile		0.1	0.2			
Unknown(m/z: 41, 45,57,71, 85, 89,149, 163)			0.3			
Methyldiphenyloxy-silane plus Dinonyl phthalate	0.3					
Dimethyl indanone	0.1		0.1			
Diethyl toluamide			0.2			
Unknown(m/z: 44, 55, 72, 86, 100, 212, 220)		0.2				
Unknown(m/z: 44, 55, 72, 86, 100, 212, 226, 429)			0.2			
C18-C23 Hydrocarbons						0.2
Dioctyl adipate + Alkylamide					0.2	
Diisopropenylbenzene	0.1					
Unknown(m/z: 43, 59, 91, 119, 161, 179, 194)			0.1			
Dodecanamide			0.1			
Tributyl citrate acetate			0.1			
Unknown (m/z: 45, 57, 73, 89, 103, 119, 145, 161, 175)				0.1		
Tetradecanoic acid amide + C24						0.1
Hexadecanamide						0.1

RGA Results and Discussion

RGA operation was conducted during each IST. During the IST-2010, the RGA was used mostly for leak checking throughout the duration of testing. In performing the leak checking, the RGA was operated

only for brief periods corresponding to when each leak-check case was being conducted. Consequently, a continuous characterization of trends in the residual gas composition was not obtained. During the IST-2011, the RGA was used for obtaining a continuous characterization of the residual gas composition over a significant portion of the test.

A portion of a typical RGA scan obtained during IST-2010 is given in Figure 12. This histogram gives relative partial pressures for the range of atomic mass from 1 to 50. The most abundant atomic mass units (AMUs) are labeled with their respective key fragments to facilitate discussion. This scan is typical of the IST-2010 data because the key fragments were seen as the major components in all the RGA data. The data indicate the presence of an air leakage. No significant amounts of lower AMU hydrocarbons are indicated. Lack of significant hydrocarbon fragments was also the case throughout the 51 to 100 AMU range. The data were taken on August 12, 2010 near the end of the IST when the pressure had reached approximately 0.5 mPa (lower 10^{-6} torr range) and had remained near this level. This is at a time when all the significant leak sources not arising from direct annulus-to-chamber avenues had been found and sealed during the course of this IST. After the existing leaks were discovered and corrected, the chamber pressure tracked in-step with the variation in annulus pressure. Thus, this indicated that only direct annulus-to-chamber leakage remained. Leakage around the large chamber doors appears to be the air source, because other major sources of possible leaks had been checked thoroughly and "fixed", if noticeable, before commencing IST-2010. Based on the low vacuum pressure obtained during the IST, chamber outgassing was considered to be a minor contributor to the vacuum pressure compared to air leakage during the latter stages of the IST. The rate of leakage was approximately 60 sccm based upon agreement of a vacuum-rate-of-rise calculation and a pumping-system-throughput calculation at the corresponding pressure.

A portion of a typical RGA scan obtained during IST-2011 is given in Figure 13. This spectrum gives relative partial pressures for the range of atomic mass from 1 to 50. These data were taken on September 28, 2011, near the end of the second IST, when the pressure had reached and maintained approximately 0.5 mPa (lower 10^{-6} torr range). Again, the most abundant AMUs are labeled with their respective key fragments to facilitate discussion. This scan is similar to the IST-2010 data and typical of an air-leak spectrum based on the principle fragments. Again, no significant amounts of lower AMU hydrocarbons are indicated. This was also the case throughout the 51 to 100 AMU range.

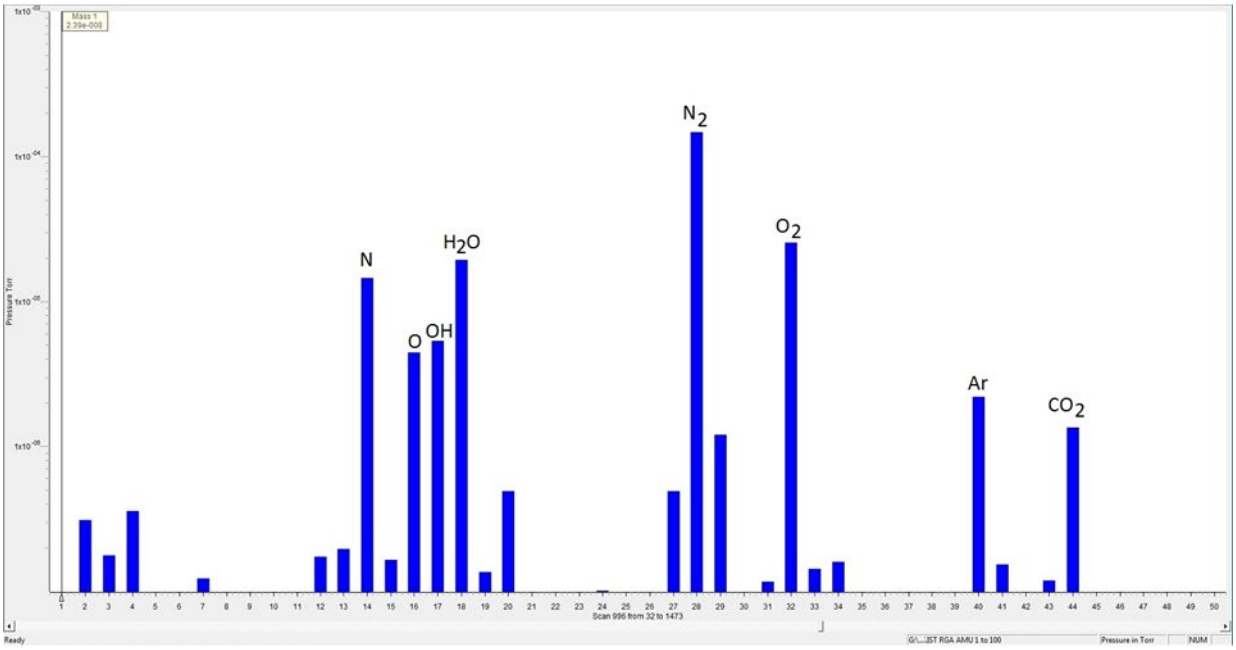

Figure 12.—IST-2010 RGA histogram spectrum.

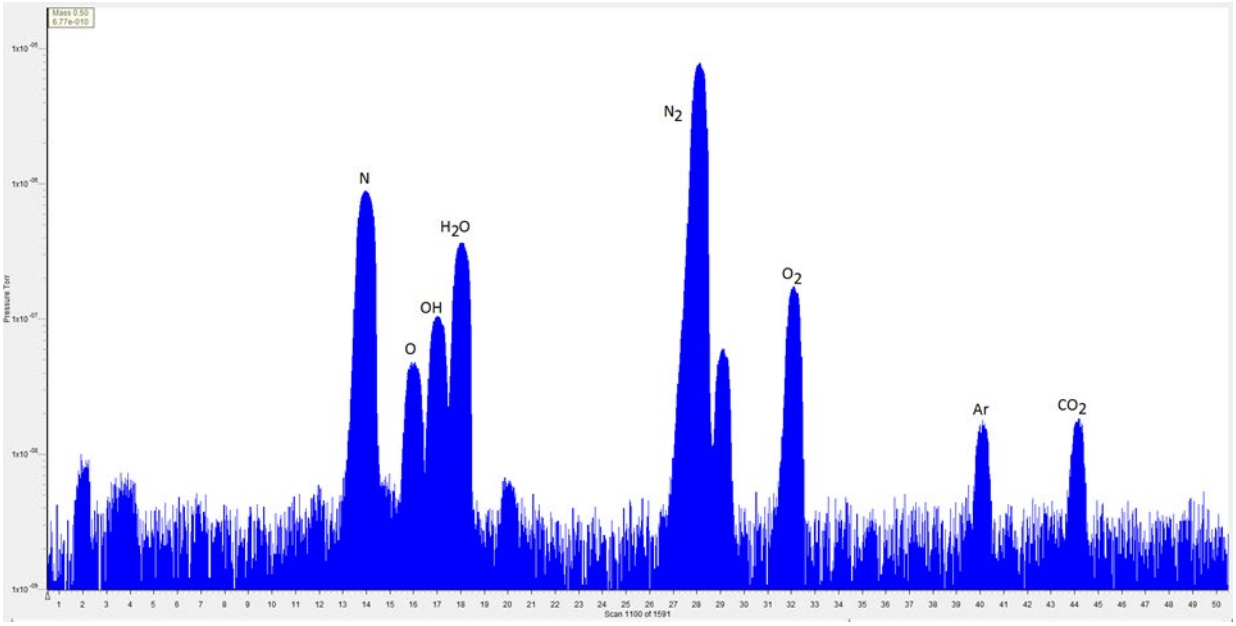

Figure 13.—IST-2011 RGA spectrum.

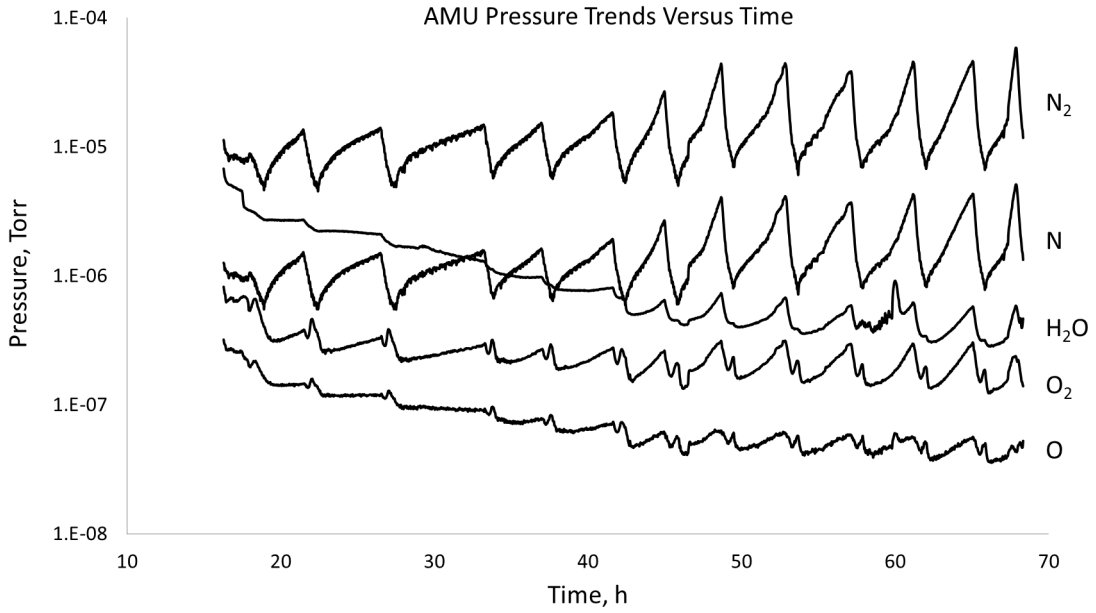

Figure 14.—IST-2011 RGA trends for main constituents.

A set of principle constituent trend lines is given in Figure 14. The time axis displayed in the figure corresponds to the time from 15:00 of September 26. This timeframe reference position is remains the case for all remaining figures relating to the IST-2011. These trend line curves reveal a number of interesting and peculiar characteristics which were manifested during IST-2011. Two characteristics that depart from expected behavior are: 1) the large oscillations in all partial pressures shown, and 2) the large rise in both molecular and atomic nitrogen partial pressures. The second characteristic clearly indicates a large nitrogen leak. For example, the typical ratio of N_2 to O_2 for air is approximately 3.7 to 1, but the ratio for the corresponding trend lines is progressively much higher than for normal air. The source of the leakage was discovered, after the IST, to be caused by an uncapped nitrogen return line that allowed cold GN_2 to be dumped into the annulus. The first characteristic is due to frequent swings in annulus pressure. Swings in pressure spanning the allowable range were much more frequent than for normal operation,

such as existed during the IST-2010. The continual GN_2 flow put an increased burden on the roughing system. A number of Beech-Russ pumps were required to be operated continuously to restrict the rate of annulus pressure rise, and when the annulus pressure approached the upper acceptable limit, a number of Roots blowers were brought on line to reduce the pressure to the lower limit. Thus, there occurred over the IST-2011 a large number of annulus pressure swings, each represented by a fast pressure drop followed by a more gradual pressure rise. The N_2-trend line and N-trend line track in phase with the annulus pressure. Additional data shows that the peaks in these two trend lines correspond with peaks in the annulus pressure, which occurs just before the additional annulus pumping is activated. The trend lines given in the last figure correspond to direct leakage between the annulus and the chamber. This was established by direct correspondence between annulus and chamber pressures, which is presented in Figure 15. Another less noticeable feature can be seen from the trend lines shown in Figure 14. The trend lines for H_2O, O_2, and O are not in phase with the two nitrogen trend lines. To reveal this phase difference, the trend lines are scaled individually so that they may be placed on a linear scale, as presented in Figure 16. Although this scaling does not preserve measured values, it allows the phase difference to become evident. The adjusted trend lines are ordered such that relative abundance is maintained. The AMUs corresponding to H_2O, O_2, O, OH, AR, and CO_2, listed here in descending order of abundance, are out of phase with the AMU corresponding to N_2. Why this is the case is discussed next.

The relative pressures of N_2 and O_2 are plotted in Figure 17, each with respect to different scales. Again, the phase difference is clearly visible, as a maximum in one component corresponds to a minimum in the other component. At all times the abundance of N_2 in the chamber is greater than the abundance of O_2. After 50 h, the ratio of a maximum in N_2 to a minimum in O_2 approached 200:1. The reason for the phase difference can be better understood by examining three tendencies. The first tendency is deduced from knowing that the nitrogen leak source was located a short distance from the inlet piping of the annulus roughing line pipe compared to the diameter of the annulus. With increased annulus pumping, the annulus pressure is decreased. A decrease in annulus pressure resulted in a disproportionate decrease in nitrogen compared to respective decreases of the minority constituents.

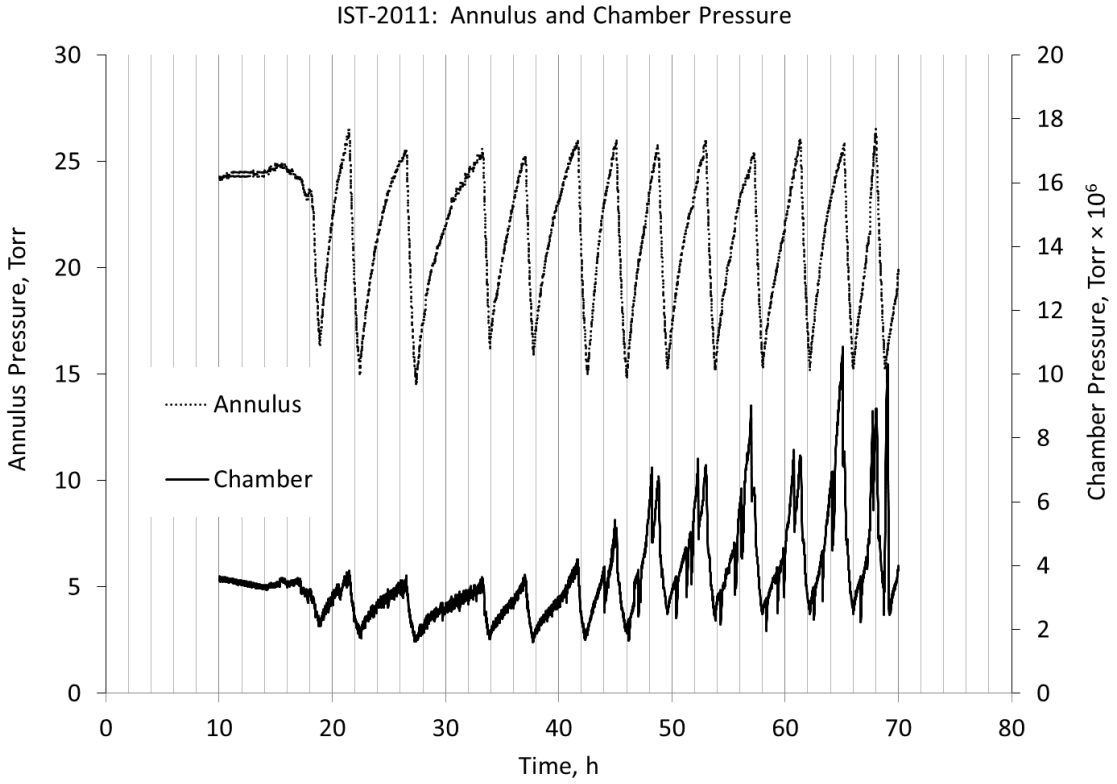

Figure 15.—Correspondence between IST-2011 annulus and test-chamber pressures.

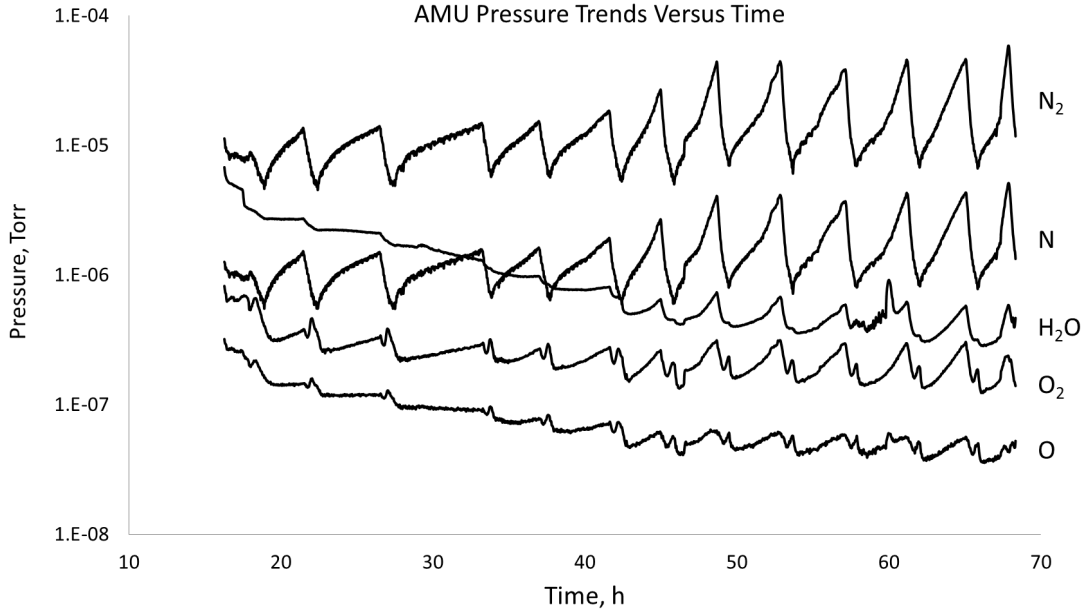

Figure 16.—IST-2011 RGA scans for several constituents. Not to scale.

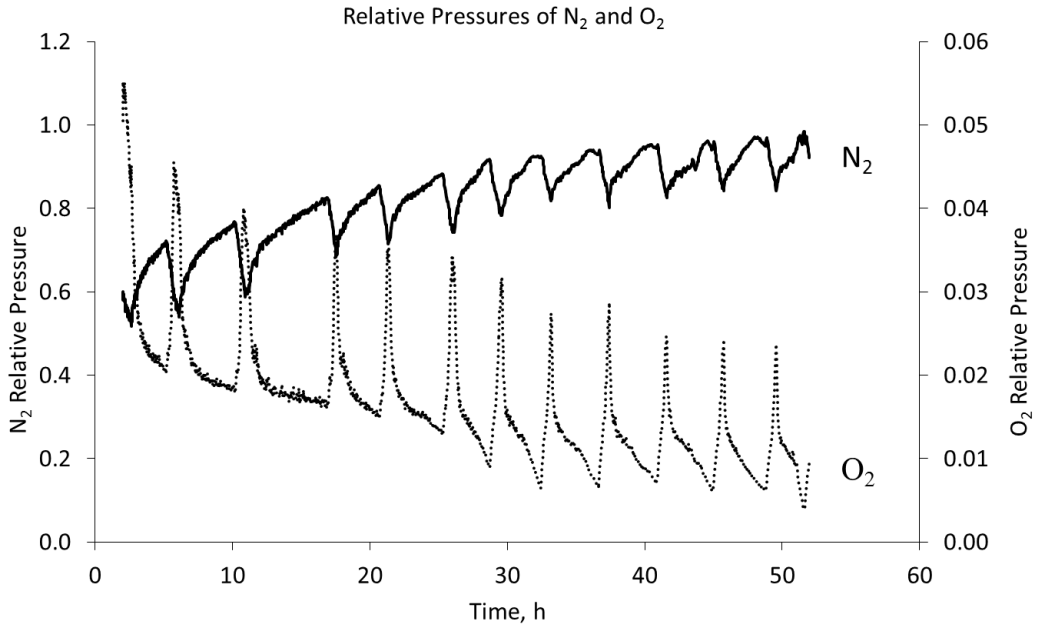

Figure 17.—IST-2011 RGA scans for N_2 and O_2 relative pressures.

The second tendency is due to the variation in outgassing with pressure. As the annulus pressure decreases, general outgassing increases. Third, the leak rate of ambient air into the annulus from outside also increases with decreasing annulus pressure. Due to these tendencies, the concentration of minority constituents increases with decreasing annulus pressure. Although total leakage to the chamber decreases as the annulus pressure decreases, the relative concentrations of the minority constituents can increase in the chamber to the extent that a given chamber partial pressure can reach a local maximum near a minimum in the total pressure. This can be seen by referring again to Figure 14, and closely examining the trend line for O_2. Figure 18 shows the trend lines for N_2 and O_2 and the quotient trend line, O_2/N_2, for a few cycles of annulus pressure. This figure clearly illustrates that as the N_2 pressures falls to a minimum, the quotient O_2/N_2 reaches a maximum. The increase in O_2/N_2 is sufficient in this case that the

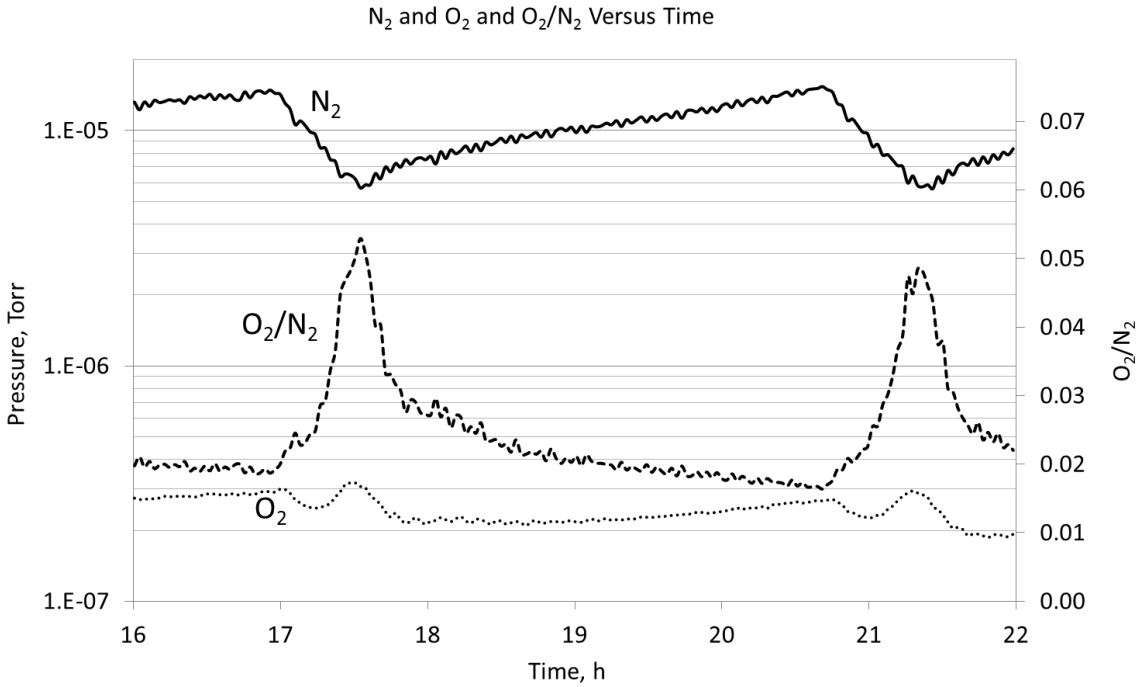

Figure 18.—IST-2011 RGA scans for N_2 and O_2 relative pressures and their ratio.

O_2 pressure reaches a maximum. Thus, a relative increase in a given annulus partial pressure, such as is the case for O_2, is sufficient to cause the leak rate of that constituent to increase even though the total leak rate is reduced due to a drop in annulus pressure. The implications of this and how it relates to chamber contamination levels is discussed in the following presentation of TQCM data.

TQCM Results and Discussion

TQCM data were taken during each IST. The data presented in Figure 19 show the variation of TQCM frequency with time over a period of 31.9 h of operation during IST-2010. The abrupt declines in frequency at each end of the curve are due to changes in the TQCM's sensor temperature. The initial decline reflects the temperature change as the TQCM finished baking out at 90 °C and approached the set temperature for operation, which was –10 °C. The final decline reflects the temperature change as the TQCM was sent again to its bake-out temperature of 90 °C to avoid condensation at the end of the high vacuum operation. The average rate of increase in frequency during the 31.9-h interval at –10 °C is 24.1 Hz/h. For the final 24 h, 8-h interval rates, given for each successive period, are as follows: 1) the first 8-h interval averaged 24.1 Hz/h; 2) the second 8-h interval averaged 22.8 Hz/h; and 3) the third 8-h interval averaged 24.3 Hz/h. The frequency rate remained very constant over the course of the run.

The data presented in Figure 20 shows the variation of TQCM frequency with time, over a period of 70.4 h of operation during IST-2011. The set temperature for operation was –10 °C, as in the previous IST. The drop in frequency seen to occur approximately 8 h into the run is due to a loose cable connection at the TQCM's controller. This cable interruption caused the sensor temperature to rise from –10 °C. The temperature rise caused the sensor to decline in frequency as accumulated contaminants desorbed. Once the cable connection was secured, the sensor obtained its operation point of –10 °C shortly afterward. While this interruption caused a sharp discontinuity in frequency, only a slight discontinuity in slope is seen. This is somewhat significant to what follows. From the point of interruption, the curve can be divided into four time intervals corresponding to whether the chamber lights were operated or were shut off. The intervals are denoted in the figure along with the slopes, which signify Hz/h, listed above the corresponding intervals. The frequencies and times corresponding to these interval endpoints are listed in

order: 1) 971 Hz at 8.22 h; 2)1073 Hz at 16.17 h; 3) 1113 Hz at 36.05 h; 4) 1154 at 42.67 h; and 5) 1182 at 70.4 h. The rates of increase in frequency during the intervals are: 1) lights on 12.8 Hz/h; 2) lights off 2.0 Hz/h; 3) lights on 6.2 Hz/h; and 4) lights off 1.0 Hz/h. As done for IST-2010 TQCM data, rates for the final 24 h, 8-h interval rates, are given for each successive period, as follows: 1) the first 8-h interval averaged 1.1 Hz/h; 2) the second 8-h interval averaged 1.0 Hz/h; and 3) the third 8-h interval averaged 0.6 Hz/h. Compared to the IST-2010 data, the rates over the last 24 h are significantly lower for the ITS-2011 data. The average rate for the final 24-h period for the IST-2011 is 0.9 Hz/h.

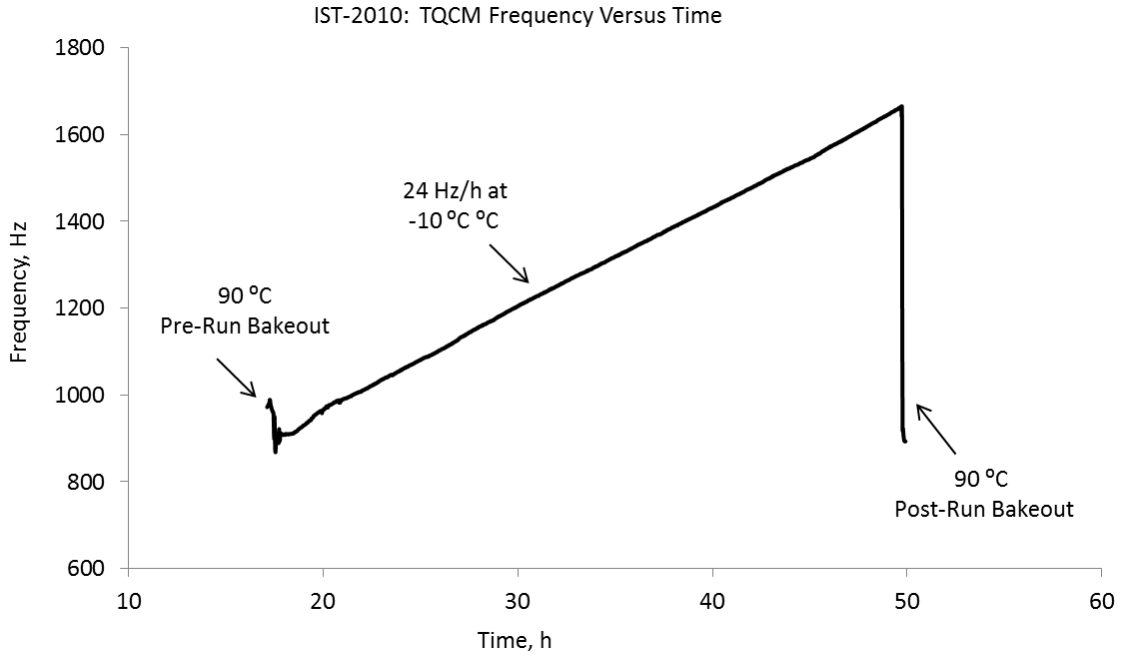

Figure 19.—IST-2010 TQCM data at –10 °C.

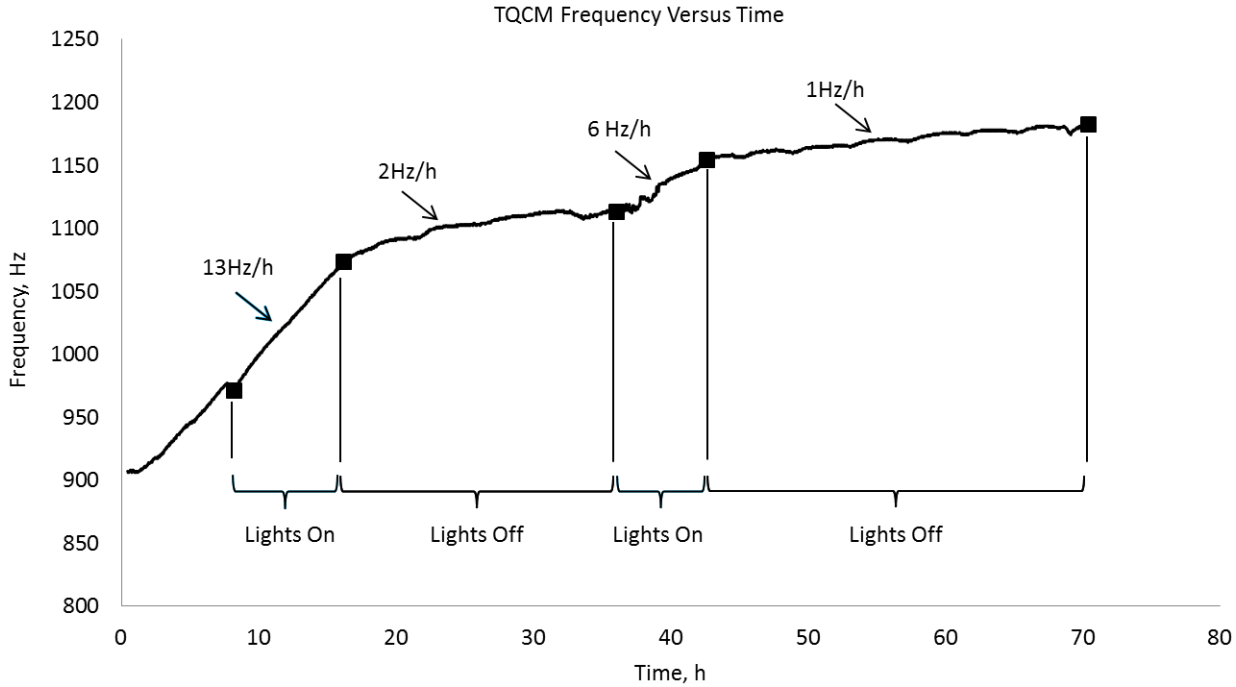

Figure 20.—IST-2011 TQCM data at –10 °C.

The contamination rates are significantly lower when the chamber lights are off. After IST-2011 was completed, this lighting effect was investigated. It was found that, before this IST, thin sheets of colored semi-transparent film had been placed in the lamp housings for visual effect purposes. During lamp operation, the film had heated and generated residue. Although the sheets of film were removed prior to IST-2011, residue remained during the IST-2011. A FTIR sample analysis of the film showed it to be polyethylene terephthalate. This substance can readily decompose with heating to produce various phthalate groups, such as those listed in Table III. The possibility is high that contaminants such as phthalates outgassed significantly when the chamber lights were operated. Such outgassing may explain the increase in the contamination rates when the lights were on.

In order to examine contamination in more detail, the last interval presented above is shown in Figure 21 with an expanded scale. In this figure, the TQCM frequency and chamber pressure are plotted on separate axes as a function of time. The major chamber pressure swings evident are due to the pressure swings in the annulus. The smaller and more frequent variations in chamber pressure were caused by an independent leak source that fluctuated with the opening and closing cycles of a scavenger system valve. The large peaks in chamber pressure occur just as the annulus pressure reaches a maximum, i.e., immediately before annulus pumping is increased. However, it can be seen by examining the cusps in the contamination curve of Figure 20 that the contamination rate increases abruptly as chamber pressure begins to decline. Conversely, the contamination rate decreases as the pressure rises, and becomes negative, forming the initial portion of a cusp, when the pressure approaches a maximum. In general, an increase in N_2 concentrations results in lower contamination rates, because the contaminant species are minority constituents, for which the concentrations decrease with increasing nitrogen concentration.

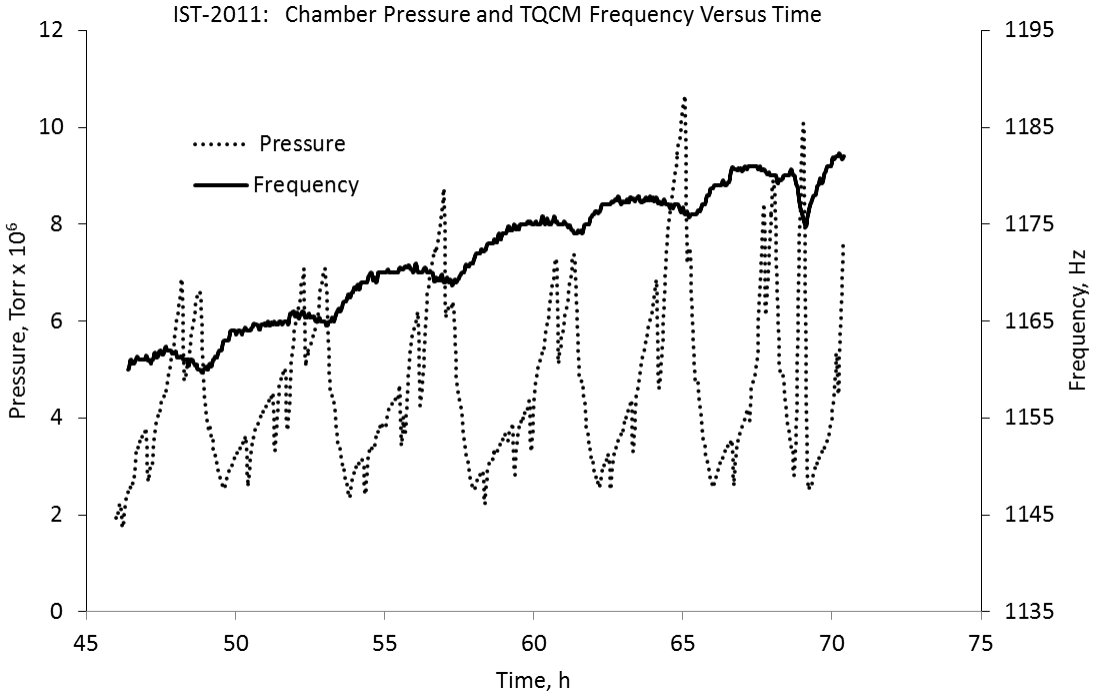

Figure 21.—Correspondence between TQCM data and chamber pressure for IST-2011.

Additional observations concerning the contamination rates are discussed. The contamination levels obtained during IST-2010 are much higher than those obtained during IST-2011. There can be several reasons for this rise. The chamber may have been cleaner entering IST-2011. This is not thought to be the case because the polar crane trolley, main hoist, auxiliary hoist, and wire ropes were installed in the chamber between ISTs. Similar preparatory cleaning was performed before both ISTs. Adding components, even non-contaminating components, to the chamber is not likely to improve overall cleanliness. The chamber lights are not likely responsible for the increased rates measured in IST-2010 for a couple of reasons. One reason is that although the chamber lights were also operated during long periods of IST-2010, they were off for other periods. However, the contamination rates remain relatively constant throughout that IST. A second reason the lights were not the likely cause of the higher rates is the polyethylene terephthalate film was placed in the lamps between the ISTs.

Assuming that the chamber cleanliness levels are similar for the two ISTs, it is feasible that the large amount of GN_2 leakage into the annulus reduced the background contamination by a significant factor, perhaps by a factor equal to 25 or more. In fact, a large factor, one as large as 25, is very plausible, when observing the decreases in the average contamination rate for common chamber lighting states for IST-2011. The rates declined from the first lights-off interval to the second lights-off interval and the from the first lights-on interval to the second lights-on interval by a factor of two for each lighting state. At this time, it is reasonable to conclude that the major influence is due to the large GN_2 leakage.

Concluding Remarks

Two high-vacuum ISTs were conducted in the SPF thermal-vacuum test chamber during the years of 2010 and 2011. The testing was performed without a cryoshroud or test article placed within the chamber. The results obtained from these two ISTs provided valuable information to form a broad characterization of chamber cleanliness.

The data also revealed a number of interesting features and unanticipated issues. For example, the annulus GN_2 leak is one issue that unexpectedly arose and established a feature to further consider for improving contamination control. The apparent reduction in contamination rates with increased GN_2 concentrations suggests that a controlled leak of nitrogen into the annulus can reduce contaminant flow into the chamber. The required amount of GN_2 can be minimalized by introducing it into minor volumes enclosing the leaks. One potential method is to “bag” recognized leak sources and flood the bags with GN_2. This method should prove quite effective around the large test chamber doors, which are particularly hard to leak check and fully seal. Operation with the test chamber enclosed allows such a flooding method to be used safely while providing effective GN_2 purging of contaminants from the bagged regions. Another unexpected issue is the evidence that chamber light operation caused contamination rates to rise appreciably above the rates obtained with the lights off during IST-2011. This increase in contamination rates could have been caused by residue originating from a terephthalate film which had temporarily been installed in the lamp housings during the time period between ISTs.

From a molecular contamination stand point, it is concluded that for vacuum testing, the chamber can be considered very clean for a wide range of test articles. RGA spectrum scans revealed no significant hydrocarbons fragments or other contaminant fragments in the range of 1 to 100 AMU. Based on molecular contamination results of NVR obtained during the ISTs without a cryoshroud in place, the chamber meets: *high* spacecraft sensitivity requirements for quantitative levels for *non-optics allowable* and *high* spacecraft sensitivity requirements for quantitative levels for *optics allowable* for IST-2011. Based on contaminant rate measurements obtained using a TQCM, the chamber exhibits a high level of cleanliness; an average rate of 0.9 Hz/h was obtained over a 24-h period at the end of IST-2011. This rate may be judged as more than satisfactory based on typical requirements. Discussions held recently with test customers having contamination-sensitive requirements indicate that levels in the range of 1 to 6 Hz/h are generally satisfactory for testing at ambient temperature.

The presence of the polar crane in the chamber during high vacuum operation has not generated any obvious intrusion as molecular contamination appears very low. Likewise, for the vacuum pumping

system, the methods now in place to mitigate backstreaming appear to be effective based on the NVR and RGA data.

Evaluating the cleanliness of the chamber with a cryoshroud in place was not considered at this time. The cleanliness of the shroud, for the operating temperature range of interest, will be the major factor in determining the level of cleanliness existing within it. The SPF test chamber has an inherent feature that works in its favor to achieve low molecular contamination rates during vacuum testing. This feature is its large size, resulting in it having the lowest area-to-volume ratio of all space simulation chambers. A given fluence (flux × time), outgassed from a unit area in a period of time, is introduced into a larger volume for lower area-to-volume ratio chambers, correspondingly producing a lower volume density. Everything else equal, it is the volume density of contaminants in the region external to the shroud that determines the transport of contaminants to the shrouds interior. A lower density proportionally lowers contaminant migration into the shroud from the surrounding volume. This same area-to-volume effect does not extend directly to contaminants originating from cryoshroud interior surface outgassing because direct shroud-to-article view-factor considerations come into play.

Additional ISTs should be considered to further characterize the chamber for cleanliness.

References

1. Rawlins, Vincent K., "Internal Erosion Rates of a 10-kW Xenon Ion Thruster," NASA TM–100954, 24th Joint Propulsion Conference, Boston, Mass. July 11-13, 1988.
2. Whalen, Margaret V., Grisnik, Stanley P., "Compatibility Experiments of Facilities, Materials, and Propellants for Electrothermal Thrusters," NASA TM–86956, 1985 JANNAF Propulsion Meeting, San Diego, Ca. April 9-12, 1985.
3. Alterovitz, S. A., Speier, H. A., Sieg, R. M., Drotos, M. N., and Dunning, J. E., "A New Technique for Oil Backstreaming Contamination Measurements," NASA TM–105312, November 1991.
4. *Product Cleanliness Levels and Contamination Control Program,* MIL-STD 1246C, April 11, 1994.
5. Tribble, A. C., "Contamination Control Engineering Design Guidelines for the Aerospace Community", NASA CR-4740, May 1996.
6. Carosso, N., "Contamination Engineering Design Guidelines," Version: Stage IV, Swales and Associates, Inc.
7. Chen, P., "Statistical Evaluation of Molecular Contamination during Spacecraft Thermal Vacuum Test," 20th Space Simulation Conference: The Changing Testing Paradigm; 35-46, (NASA/CP—1999-208598), Feb. 1999.

REPORT DOCUMENTATION PAGE	Form Approved OMB No. 0704-0188

1. REPORT DATE *(DD-MM-YYYY)*	2. REPORT TYPE	3. DATES COVERED *(From - To)*
01-12-2012	Technical Memorandum	

4. TITLE AND SUBTITLE
Contamination Control Assessment of the World's Largest Space Environment Simulation Chamber

5a. CONTRACT NUMBER

5b. GRANT NUMBER

5c. PROGRAM ELEMENT NUMBER

6. AUTHOR(S)
Snyder, Aaron; Henry, Michael, W.; Grisnik, Stanley, P.; Sinclair, Stephen, M.

5d. PROJECT NUMBER

5e. TASK NUMBER

5f. WORK UNIT NUMBER
WBS 359257.01.07.01

7. PERFORMING ORGANIZATION NAME(S) AND ADDRESS(ES)
National Aeronautics and Space Administration
John H. Glenn Research Center at Lewis Field
Cleveland, Ohio 44135-3191

8. PERFORMING ORGANIZATION REPORT NUMBER
E-18572

9. SPONSORING/MONITORING AGENCY NAME(S) AND ADDRESS(ES)
National Aeronautics and Space Administration
Washington, DC 20546-0001

10. SPONSORING/MONITOR'S ACRONYM(S)
NASA

11. SPONSORING/MONITORING REPORT NUMBER
NASA/TM-2012-217823

12. DISTRIBUTION/AVAILABILITY STATEMENT
Unclassified-Unlimited
Subject Category: 14
Available electronically at http://www.sti.nasa.gov
This publication is available from the NASA Center for AeroSpace Information, 443-757-5802

13. SUPPLEMENTARY NOTES

14. ABSTRACT
The Space Power Facility's thermal vacuum test chamber is the largest chamber in the world capable of providing an environment for space simulation. To improve performance and meet stringent requirements of a wide customer base, significant modifications were made to the vacuum chamber. These include major changes to the vacuum system and numerous enhancements to the chamber's unique polar crane, with a goal of providing high cleanliness levels. The significance of these changes and modifications are discussed in this paper. In addition, the composition and arrangement of the pumping system and its impact on molecular back-streaming are discussed in detail. Molecular contamination measurements obtained with a TQCM and witness wafers during two recent integrated system tests of the chamber are presented and discussed. Finally, a concluding remarks section is presented.

15. SUBJECT TERMS
Space; Contamination; Thermal; Vacuum; Spacecraft

16. SECURITY CLASSIFICATION OF:			17. LIMITATION OF ABSTRACT	18. NUMBER OF PAGES	19a. NAME OF RESPONSIBLE PERSON
a. REPORT	b. ABSTRACT	c. THIS PAGE			STI Help Desk (email:help@sti.nasa.gov)
U	U	U	UU	32	19b. TELEPHONE NUMBER *(include area code)* 443-757-5802